

Article

Black Quartz from the Burano Formation (Val Secchia, Italy): An Unusual Gem

Franca Caucia ^{1,*}, Maurizio Scacchetti ², Luigi Marinoni ¹ and Mattia Gilio ¹¹ Earth and Environmental Sciences Department, University of Pavia, Via Ferrata 1, 27100 Pavia, Italy² A.M.I. (Associazione Micromineralogica Italiana), 80100 Naples, Italy

* Correspondence: caucia@crystal.unipv.it

Abstract: The Burano Formation in Val Secchia in the province of Reggio Emilia is rich in black or very dark quartz. The crystals are often pitted by scars, rarely shiny, often opaque, rarely translucent, and about 3 cm long. However, they have a beautiful color and are generally euhedral and bi-terminate with simple habitus and well developed faces—for these characteristics, they are very sought after by collectors. Micro-Raman analyses showed the quartz contains abundant inclusions of anhydrite and graphite. The inclusions of anhydrite are responsible for the chromatic inhomogeneity, while the black color is linked to the presence of disordered graphite inclusions. LA-ICP-MS analyses did not show a significant presence of chromophore elements. Black quartz formed in the original evaporite deposits of gypsum, which, due to diagenesis and the increase in temperature during deep tectonic burial conditions, lost water of crystallization and subsequently transformed into anhydrite. After the formation of quartz crystals, the Burano Formation was exhumated and rehydrated, resulting in gypsification at conditions close to the surface. The black quartzes of the Burano Formation represent an appreciable gemological material for the development of local craftsmanship, even if the difficulties in reaching the deposit limit their marketing.

Keywords: Burano Formation; black quartz; disordered graphite inclusions; gemstone; Raman spectrometry



Citation: Caucia, F.; Scacchetti, M.; Marinoni, L.; Gilio, M. Black Quartz from the Burano Formation (Val Secchia, Italy): An Unusual Gem. *Minerals* **2022**, *12*, 1449. <https://doi.org/10.3390/min12111449>

Academic Editors: Stefanos Karampelas and Emmanuel Fritsch

Received: 4 August 2022

Accepted: 14 November 2022

Published: 16 November 2022

Publisher's Note: MDPI stays neutral with regard to jurisdictional claims in published maps and institutional affiliations.



Copyright: © 2022 by the authors. Licensee MDPI, Basel, Switzerland. This article is an open access article distributed under the terms and conditions of the Creative Commons Attribution (CC BY) license (<https://creativecommons.org/licenses/by/4.0/>).

1. Introduction

Black or dark colored quartzes are widespread in nature, are called by different names, and are generally appreciated in the market for their gemological properties [1]. The most popular variety of black quartz is called "smoky": its color varies from gray to black and is due to the presence of color centers produced by radiation (natural or artificial) and by Al ions in its crystal lattice. If the smoky quartzes are heated to around 260–300 °C, they turn into hyaline quartz as the color centers are deactivated with the temperature [1–4]. The most beautiful smoky quartzes, even from a commercial point of view, come from the United States and are often associated with milky quartz; in particular, they are found on Mount Apatite (Auburn, Maine), in Coos County (New Hampshire), and in Arkansas [1,5]. However, there is also another type of quartz that shows a more or less dark color (from very dark grey to black), which is not due to color centers but to the presence of inclusions of carbonaceous or bituminous organic substances. If rubbed or broken, these quartzes emit a characteristic odor and are generally opaque. This type of quartz abounds in numerous outcrops in the Apennines in the Emilia Romagna region of Italy [1,2,6,7]. These quartzes are more generically called black quartz and non-smoky quartz [1,2].

In this work, we studied black quartz samples from two outcrops in the formation of Burano in Val Secchia in the northern Apennines near the city of Reggio Emilia (Italy). They have been little investigated, although they are suitable for commercialization due to their good gemological characteristics (color, diaphaneity, and hardness). These quartzes are also known for providing a beautiful aesthetic effect of chromatic contrast with the rocks that

contain them [2]. The Reggio Emilia province is also rich in other minerals used in jewelry, such as datolite and prehnite, that occur in the ophiolitic lithologies scattered in the chaotic clays, and hyaline quartz, which is found in the sandstones of the upper Apennines [2]. In this work, we examined the geological context and the geochemical, mineralogical, and gemological characteristics of the black quartz to understand their genetic conditions and the causes that give the mineral its color. In particular, our work has mainly focused on the characterization of the inclusions present in these quartzes. In quartz, different types of inclusions with liquid, gaseous, or solid components are frequently found, sometimes even combined with each other [2]. The study of their composition provides important information on the genesis and physical properties, such as color, of the host minerals.

2. Geological Setting

The lithologies that include black quartz are part of the Tuscan Nappe that is the sedimentary succession deposited in the most proximal portion to the European continental margin. The Tuscan Nappe is partially covered by other nappes, like Cervarola, Modino, and Ligurian Units, and its basal sequence consists of the Triassic evaporitic Burano Formation [8–12] (Figure 1). This formation is mainly composed of the alternation of gypsum-anhydrite rocks ranging in size from meters to decameters, and dark gray dolomitic limestones; at a depth, there are also rock salt crystals, not observable on the surface [13–16] (Figure 2).

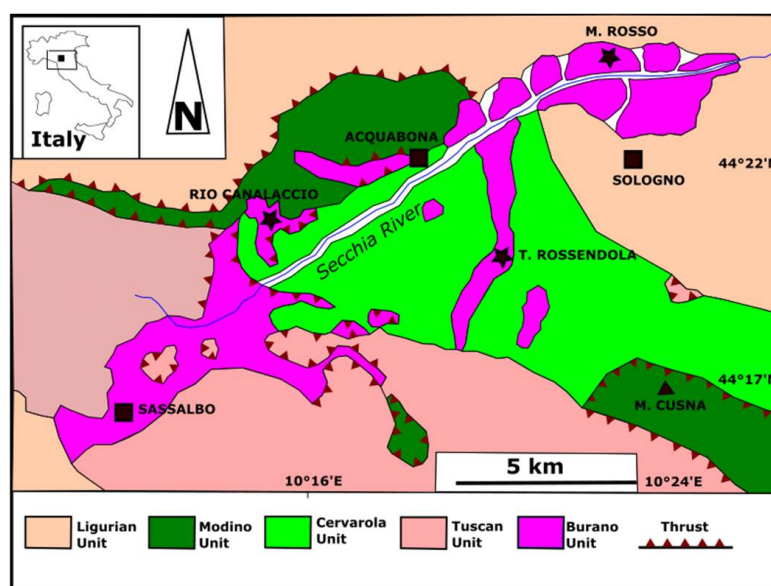


Figure 1. Simplified geological map of the upper Apennines of Reggio Emilia province with the Triassic Burano Formation; the black stars indicate the sites of the studied samples. Map redrawn from [13].

These evaporitic rocks are very soluble, and, consequently, widespread karst phenomena such as sinkholes, aquifers, and saline springs are observed along the banks of the Secchia river and its tributary Ozola [14,17–19]. Near Reggio Emilia, the Burano Formation reaches a thickness of 2200 m and has been interpreted as a transpressive system, transversal to the main tectonic lines of the northern Apennines [20,21]. During a deformation phase in the Miocene, there was a disruption in thrust slices and inclusion in younger allochthonous units [22,23]; as a consequence, the outcrops along the Secchia and Ozola valleys are subjected to widespread phenomena of instability such as massive landslides (Figure 3).

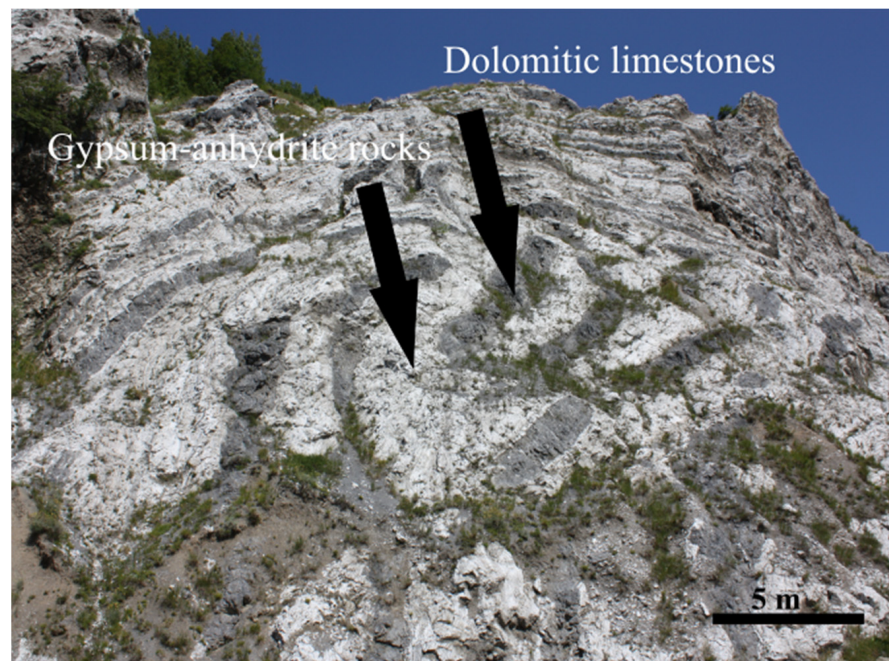


Figure 2. Spectacular outcrop of the Burano Formation in Val Secchia near Sassalbo, (Massa province, Tuscany) where you can observe the alternation of lighter colored levels of gypsum-anhydrite and darker levels of dolomitic limestones. Black quartzes are found mainly in anhydrite levels.



Figure 3. Southern slope of Mt. Rosso outcropping along River Secchia Valley, with widespread phenomena of instability.

The mineralogical composition of the Burano Formation consists mainly of gypsum, quartz, sulfur, aragonite, calcite, dolomite, barite, celestine, magnesite, fluorite, and pyrite [2,16]. (Figure 4).

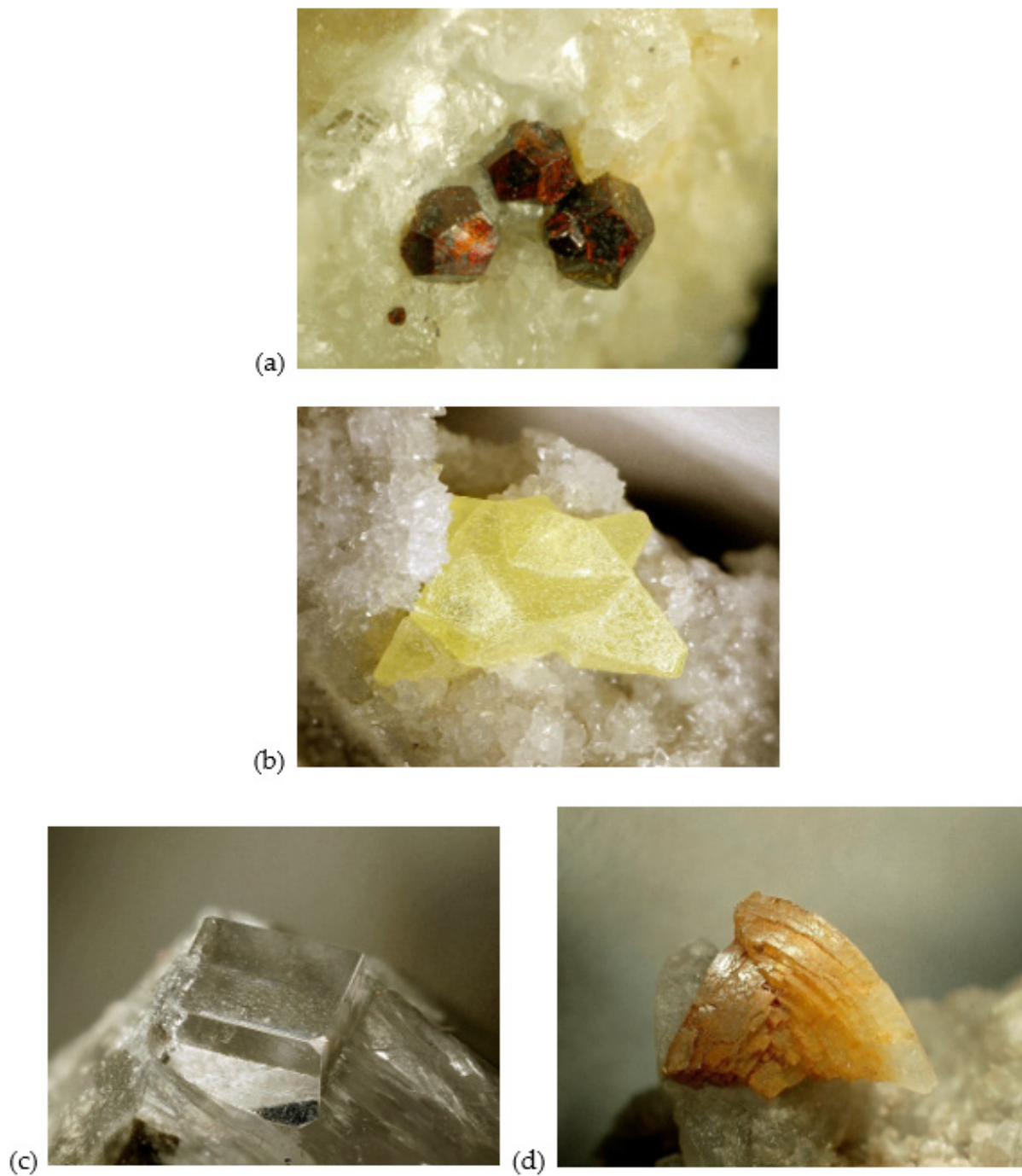


Figure 4. Minerals from the Burano Formation: (a) pyrite from Mt. Rosso (0.6 mm length); (b) sulfur from Rio Biola (Reggio Emilia, Italy), 5.3 mm; (c) fluorite from Sassalbo (Massa province), 2.1 mm; and (d) dolomite from Rio Canalaccio, Reggio Emilia, 3.9 mm. Photos by Enrico Bonacina.

The black quartz crystals are found exclusively in some levels of anhydrite and gypsum that never exceed two meters in thickness and emerge for a few tens of meters (Figure 5).

At the top of the reliefs where the Burano Formation outcrops, the meteoric water has dissolved the evaporitic rocks, releasing the black quartz crystals incorporated in them, and consequently the crystals are found isolated in the eluvial soils of these areas.



Figure 5. Anhydrite levels with black quartz crystals, from Mt. Rosso.

3. Materials and Methods

About 350 euhedral black quartz crystals, ranging in size from 2 to 30 mm, were sampled by M.S. or gifted by local collectors and were used for morphological study. Standard gemological analyses were performed on five gems (3.54–14.54 ct weight) cut from rough samples, to describe optical properties, specific gravity, and ultraviolet fluorescence. Density was measured using a Presidium PCS100 Sensible hydrostatic balance, and the color was evaluated with an RGB (red, green, blue) [24] color table method. The refractive index was measured with the distant vision method using a Kruss refractometer (1.45–1.80 range) and a contact liquid with an RI of 1.80. Ultraviolet fluorescence was investigated with a shortwave (254 nm) and long-wave (365 nm) UV lamp (Power 3W 20 cm distance of observation). Micro-Raman scattering measurements were conducted with a Horiba Jobin Yvon Explora Plus single monochromator spectrometer (grating of 2400 groove/mm), equipped with an Olympus BX41 microscope. The analyses were conducted on the inclusions previously observed under the microscope, to better understand their mineralogical composition. Raman spectra were recorded with 532 nm excitation. The spectrometer was calibrated to the silicon Raman peak at 520.5 cm^{-1} . The spectral resolution was $\sim 2\text{ cm}^{-1}$, and the instrumental accuracy in determining the peak positions was approximately 0.56 cm^{-1} . Raman spectra were collected in the spectral range $100\text{--}4000\text{ cm}^{-1}$ for 5 seconds, averaging over 40 scans accumulated. Trace elements were determined by laser-ablation inductively coupled plasma mass spectrometry (LA-ICP-MS) at the IGG-CNR Laboratory of Pavia, combining an excimer laser (193 nm; Lambda Physik with GeoLas optics) with a triple quadrupole ICPMS (QQQ Agilent 8900). The analyses concerned the whole samples of quartz. The laser was operated at a repetition rate of 10 Hz, with a fluence of $6\text{ J}\cdot\text{cm}^{-2}$ and an ablation spot size of $55\text{ }\mu\text{m}$. The optimization of LA-ICP-MS to minimize elemental fractionation was performed by ablating NIST 612 glass and adjusting the nebulizer Ar and the carrier laser cell He gas flows to obtain the ratio of ^{232}Th and ^{238}U signals close to 1, by minimizing the ThO^+/Th^+ ratio ($<1\%$) in order to reduce the formation of polyatomic oxides. The selected masses were acquired in MS/MS mode, and each analysis consisted of the acquisition of 1 min of background before and after about 1 min of ablation signal. Data reduction was performed with the “GLITTER” software package [21], using NIST SRM 610 glass as an external standard and ^{29}Si as an internal standard, changing the value in each analysis as from microprobe. Precision and accuracy estimated on the USGS basaltic glass standard BCR2 and NIST612 were better than 10%. Three spots per sample were measured.

4. Results

4.1. Morphology

The quartz crystals of the Burano Formation exhibit some dimensional (Figure 6) and chromatic variability: few crystals are very light grey or grey (Figure 7a), while most, particularly those examined in this work, have a black opaque color and a waxy, sometimes greasy luster (Figure 7b). Many crystals appear bi-terminated with well-developed faces (Figure 7c); they more frequently show a prismatic habit, formed by the combination of an apparently hexagonal prism (actually the combination of two trigonal prisms) with two rhombohedrons (one positive and one negative) often twinned and equally developed to simulate a hexagonal bipyramid. Sometimes the faces of the rhombohedrons are much extended and cover the faces of the prism—in this case, the crystal takes on an almost bipyramidal habit (Figures 6 and 7d). Shortened and squat crystals are also observed, and some appear disproportionate or deformed. Few samples have a twinning according to the law of Japan [25], in which two flat crystals are attached to each other with the main axes arranged at $84^{\circ} 33'$.

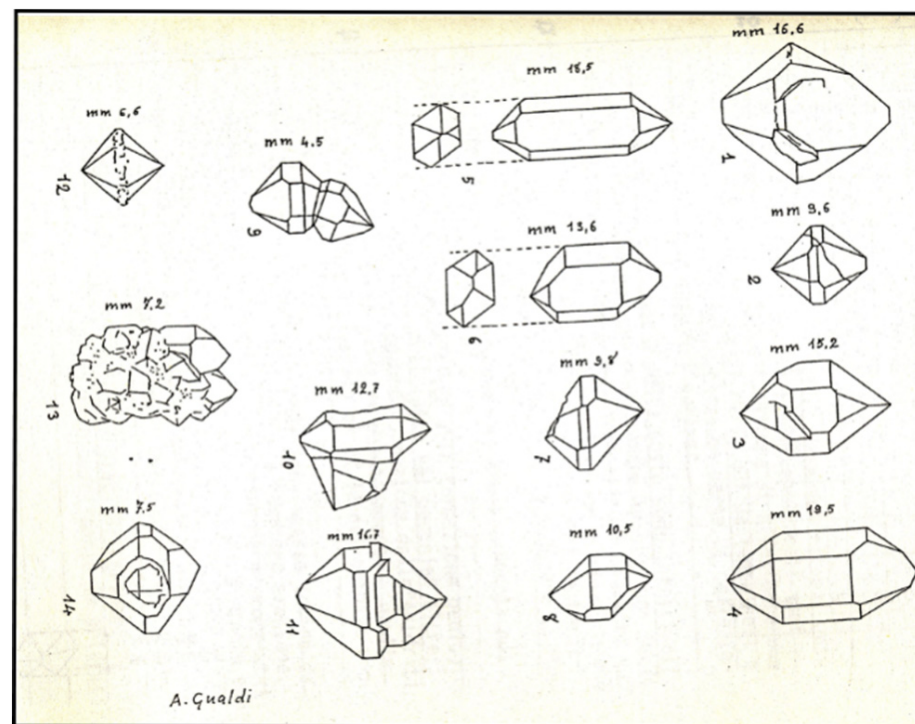


Figure 6. Morphological table of Burano Formation quartz (drawn by Alberto Gualdi).

The minimum values of length and width of 355 crystals from the Burano Formation were measured with a micrometer; the values are shown on the diagram of Figure 8 (black spots). Since the minimum length/width ratio (L/W) is directly proportional to the length of the prism, its values can be used to describe the type of habitus. The L/W ratio is a very important parameter for gem cutters who use it frequently to determine the correct patterns for cutting gemstones and also create new gem designs. The values of the L/W ratio slightly higher than 1 correspond to type III, i.e. a habitus without a prism, while the values of the L/W ratio of about 2.5 correspond to type VI, with a fairly well developed prism [26,27].

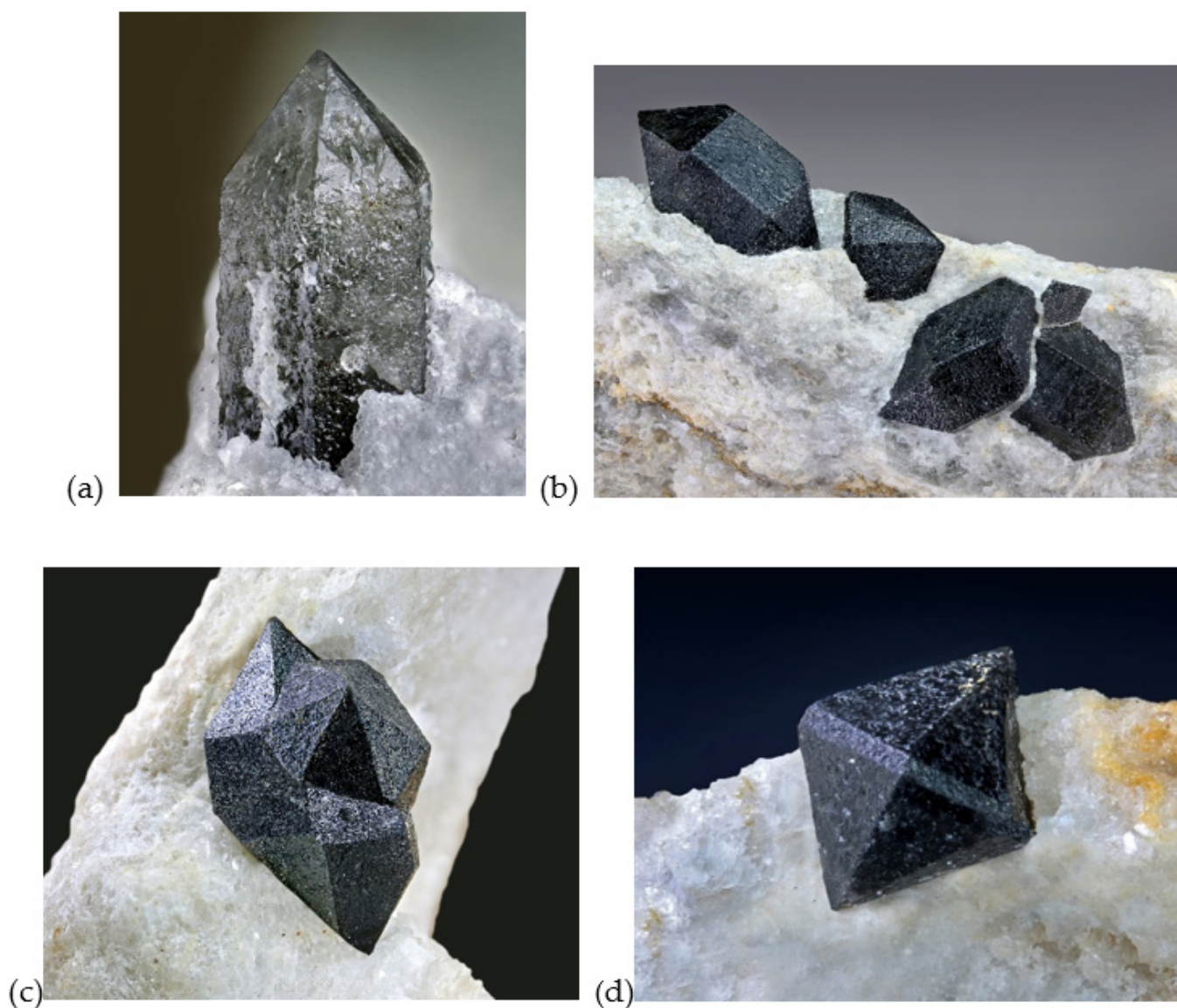


Figure 7. Quartz crystals of the Val Secchia (Monte Rosso) gypsum rock formation: (a) grey: length 15 mm; (b) black: length of the crystal on the left 30 mm; (c) black: length 32 mm; (d) black: length 30 mm. Note the rough surface due to the imprints of the white anhydrite crystals. Photos by Antonio Miglioli.

No close correlations are observed between crystal type, size, and color; but crystals longer than 1 cm with an L/W ratio of about 2 are more frequently black, while those of type III shorter than 1 cm are more frequently gray. On the contrary, a closer correlation between the color of the crystals and their location is observed, as black crystals are almost exclusively present in some anhydrite layers in the eastern outcrops of the Burano Formation. The shapes of the black quartzes of the Burano Formation are mainly prismatic-hexagonal, and the L/W ratio varies only between 1.17 and 3. For comparison purposes, the values for quartz crystals from the Alps (Val Veny, Triolet, and Ayas in Aosta Valley; Reale in Formazza Valley; and Dosso dei Cristalli in Malenco Valley) are also reported (blue spots). The quartz crystals present in the cracks of the rocks of the Alps often show a typical rhombohedral shape, very elongated and pointed. In the diagram of Figure 8 we have plotted the values of W and L of about one hundred crystals collected by M.S. in various Alpine locations; we observe that most of the crystals have an index $L \gg 3$ (blue spots).

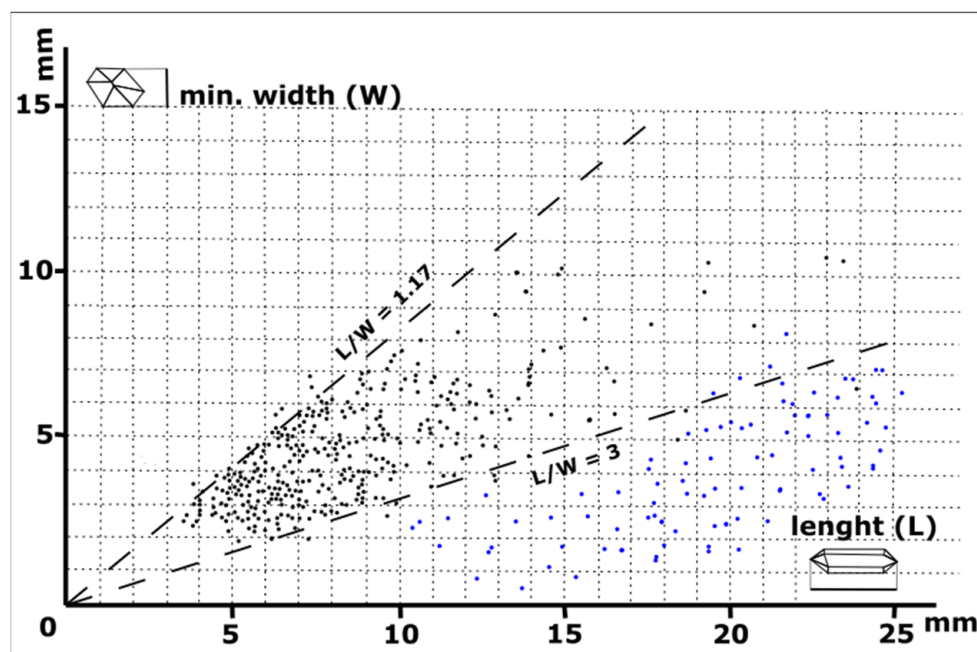


Figure 8. Diagram of length vs. minimal width on 355 crystals from the Burano Formation (black spots) and 104 hyaline quartz crystals from Alps (blue spots).

4.2. Gemological Results

Quartz crystals can be faceted even if included—in fact none of our crystals broke during cutting. Sometimes, since the crystals have a nice euhedral morphology, it is preferable to use the simple shapes already present and carry out only the polishing or regularization of any anomalous faces. The surfaces of the crystals are often pitted by the encasing rock and have high luster; the crystals are usually opaque (Figure 9).

Table 1. Gemological properties of black quartz from the Burano Formation.

Sample	Dimensions (mm)	Weight (ct)	Cut	Shape	RI	Specific Gravity	Color (RGB)
1	12 × 9 × 4	3.54	Cabochon	Pear	1.542; 1.550	2.661	Black
2	11 × 11 × 5	5.72	Cabochon	Round	1.546; 1.553	2.651	Black
3	12 × 9 × 6	5.83	Cabochon	Oval	1.544; 1.552	2.643	Black spots grey
4	19 × 15 × 9	14.54	Fancy	Hexagonal	1.543; 1.552	2.650	Black spots grey
5	14 × 12 × 6	6.11	Fancy	Rhomboid	1.542; 1.551	2.640	Black spots grey

The faceted specimens have vivid, intense, and rich colors, ranging from homogeneous black to black with grayish spots, and are of gemological interest. The luster is vitreous; the diaphaneity is opaque. The gems were cut from specimens with a form resulting from a combination of hexagonal prisms and hexagonal bipyramid (Figure 10).

The physical and optical properties of the investigated gems are reported in Table 1.

The specific gravity ranges from 2.643 to 2.661; the refractive indexes between 1.542–1.548 and 1.550–1.553 (using spot analysis and turning the sample), in agreement with the literature data for similar quartz. All the analyzed gems are inert to long and short UV.



Figure 9. Quartz round cabochon (diameter 11 mm, Table 1, sample 2) with small veins of anhydrite. Photo by Enrico Borghi.

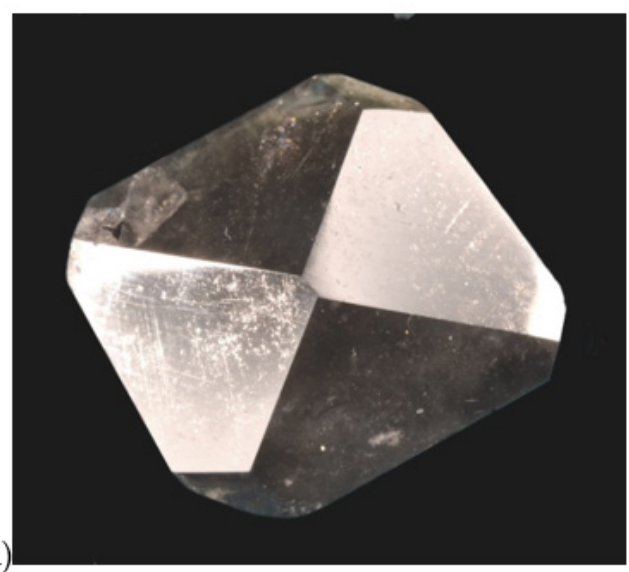
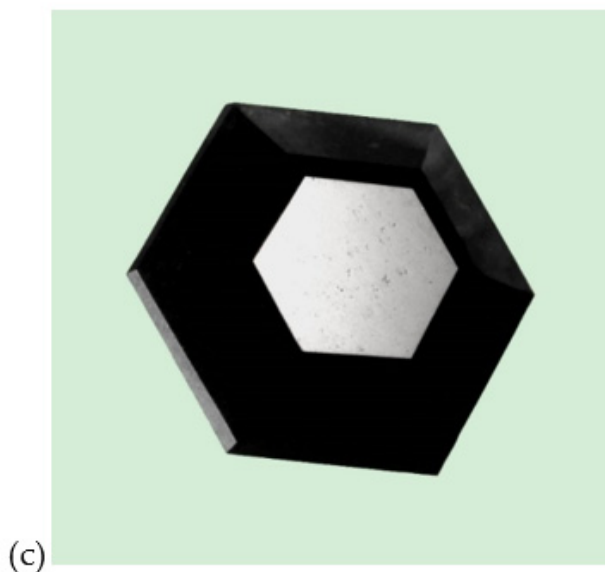
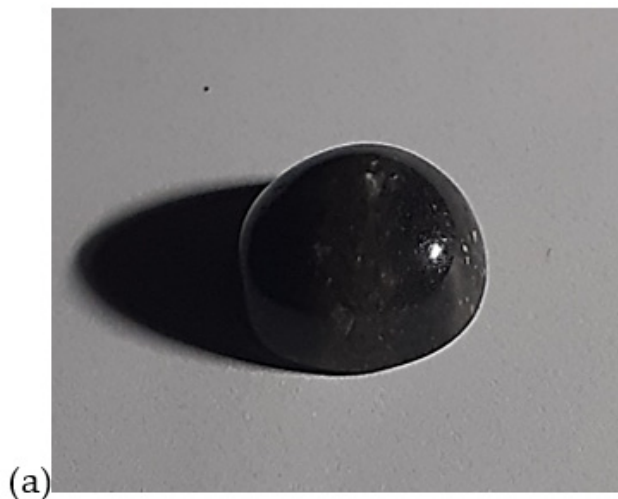


Figure 10. (a) Oval cabochon (length 12 mm, sample 3); (b) pear cabochon (length 12 mm, sample 1); (c) fancy black quartz (length 8 mm, sample 4); and (d) fancy black quartz (length 14 mm, sample 5). Photo by Enrico Borghi.

4.3. Raman Results

Raman analyses on quartz and inclusions (gemstone n. 2) were carried out to confirm that the color is actually due to the presence of graphite. Since the attempts on cabochon gems were unsuccessful, we performed the analysis on a thin section of the sample; however, given that the analyzed inclusions are not superficial but completely incorporated in the quartz, we believe it is unlikely that the polishing operation has altered the quality of the analyses. The Raman analyses of quartz and relative inclusions were carried out on a thin petrographic section of gem 2 in order to confirm that the color is linked to graphite (Figure 11).

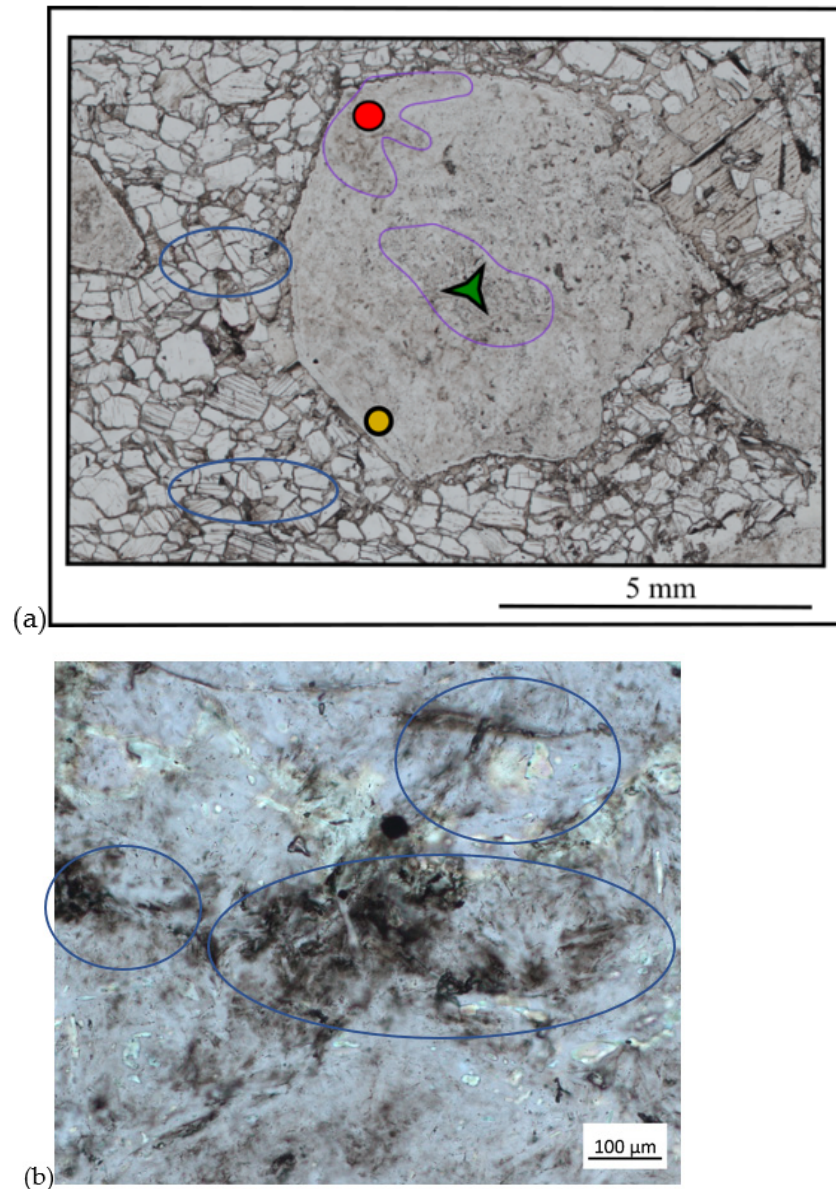


Figure 11. Cont.

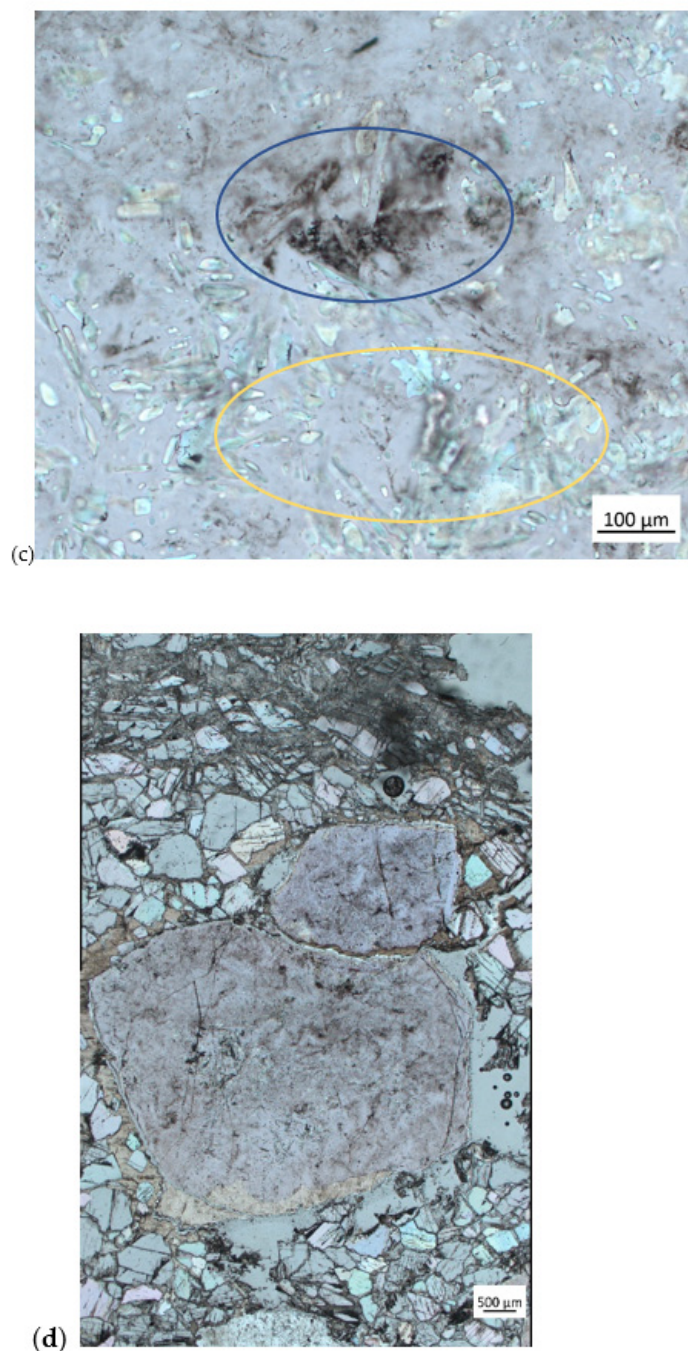


Figure 11. (a) petrographic thin section with disordered graphite (red circle), anhydrite (green star), and bukovskyite (orange circle) inclusions incorporated into the quartz. Inside the host rock there are also (b) gypsum crystals (blue ovals); (c) graphite (blue ovals) and anhydrite (yellow ovals) inclusions clusters (20 \times); and (d) dark spots, all of graphite clusters (2.5 \times).

In Figure 12 we report the Raman analysis spectra of four points (red color), which highlight the presence of anhydrite, bukovskyite, and disordered graphite, together with the host quartz, and the relative RRUFF database spectra (grey color). According to [28], the bending of Si–O–Si bond angles and twisting are localized below 300 cm^{-1} (126, 206, and 263 cm^{-1} in Figure 12c), and the bending of O–Si–O angles are localized in the region 350–500 cm^{-1} (395, 465 cm^{-1} in Figure 12c). According to [29,30], in the sulfate group vibrational modes of Ca–O bonds appear in Raman spectra in the region below 400 cm^{-1} . In Figure 12 the bands at 140 and 160 cm^{-1} are due to the vibration of Ca–O

bond. The bands at 416 , 508 cm^{-1} and 612 , 628 , 680 cm^{-1} are assigned respectively to the symmetric and antisymmetric bending SO_4 . The band at 1020 is due to the symmetric stretching SO_4 . The peak at 1160 is due to the antisymmetric stretching SO_4 stretching mode. Along the edge of the quartz was recognized the bukovskyite [29], a powdery micro-crystalline aggregates of metacolloidal material, commonly associated with gypsum and kankite (Figures 11 and 12b). According to [31], the band at 814 cm^{-1} is assigned to the antisymmetric stretching of AsO_4 ; the bands at 984 and 1010 , 1131 cm^{-1} are due to the symmetric and antisymmetric stretching of SO_4 , respectively. The band at 1652 cm^{-1} is assigned to the H_2O bending vibration. Raman spectroscopy also made it possible to evaluate the degree of crystallinity of the graphite inclusions [32]. The crystal lattice of graphite consists of an ordered stacking of planes within which the C atoms are organized in hexagonal rings, forming a honeycomb structure. The crystal structure of hexagonal graphite corresponding to the space group $P63/mmc$ is realistic only for the case of an ideal single crystal. The decrease in the size of the crystalline domains leads to a decrease in the degree of order, which is greater in nanocrystalline graphite where the lattice planes are distorted and often formed by rings with an odd number of atoms. The exact interpretation of the position and shape of the graphite bands depends on several factors, such as the excitation of the laser, the orientation, and the resolution [32]. The 1581 cm^{-1} frequency band is related to a C-C vibration stretching of the individual planes and is common to all the different forms of carbon that have sp^2 hybridized atoms. As the size of the crystalline domains decreases, a further broad band (not present in the monocrystalline graphite) is observed at about 1350 cm^{-1} (1340 cm^{-1} in Figure 12d), which indicates the presence of structural defects such as the deformations of the planes due to the small size of the crystal. Raman spectra of graphite show that the increase in crystallinity is accompanied by the disappearance of the band at about 1350 cm^{-1} . The peak at 1620 cm^{-1} (see Figure 12d) due to the antisymmetric translation motion is characteristic of polycrystalline graphite alone [33–36].

4.4. LA-ICP-MS Results

LA-ICP-MS analyses concerned the whole samples of five quartz; the results are reported in Table 2. We observe that the investigated quartz has low contents of trace elements; in fact, the Si–O bonds in quartz have a very stable atomic configuration so that only small amounts of other chemical elements can enter the structure of this mineral. In some cases, however, some trace elements, vicariant or interstitial, can enter the quartz structure either by replacing the Si or by entering the channels that run parallel to the c axis [1].

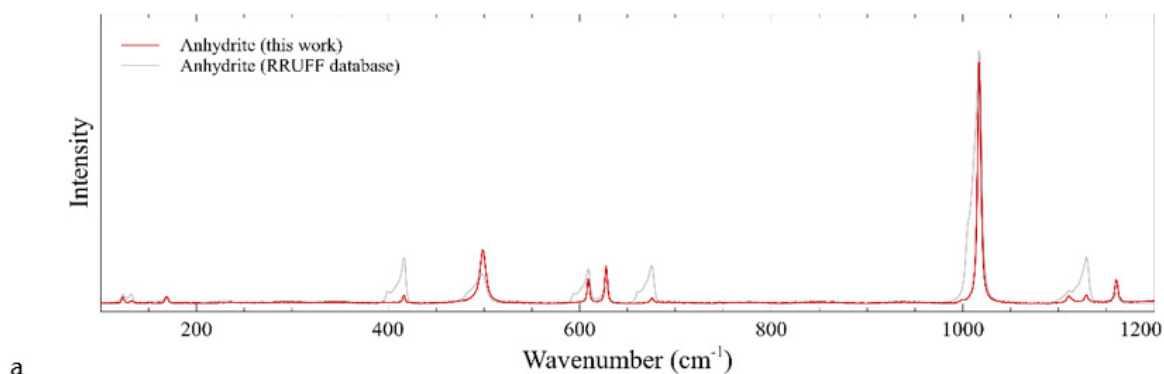


Figure 12. Cont.

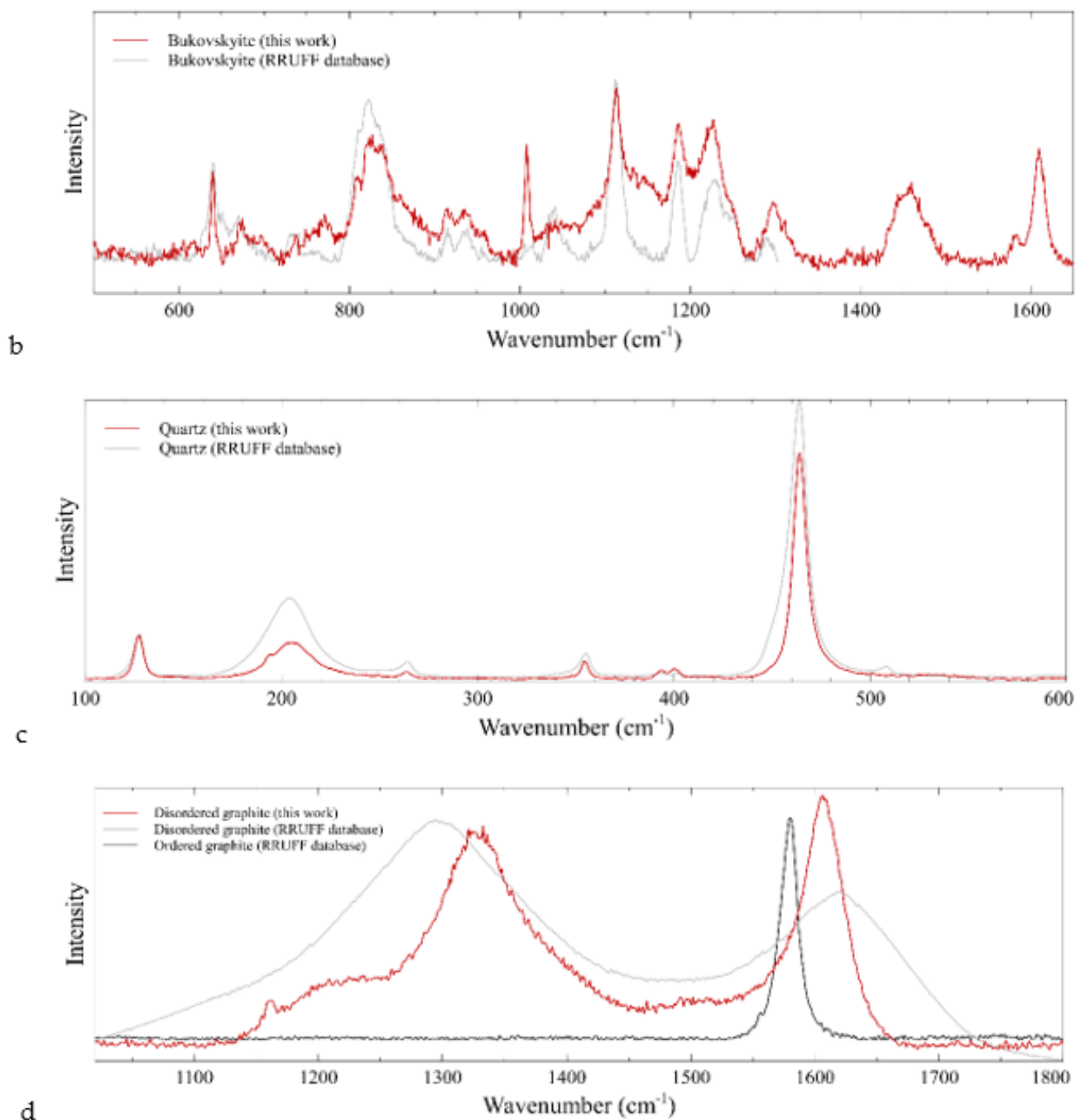


Figure 12. The Raman spectra of this work (red color) and the relative RRUFF database (grey color): (a) Raman spectra of anhydrite (416, 508, 612, 1129 cm⁻¹) [29,30,37]; (b) bukovskyite (814, 984, 1010, 1131, 1652 cm⁻¹) [29]; (c) quartz (128, 206, 263, 356, 465 cm⁻¹) [28,38]; and (d) disordered graphite (1340, 1620 cm⁻¹) [32,39] (Sample 2).

The most abundant element in the analyzed quartz is Al (194–352 ppm), followed by lower contents of Hf (26–90 ppm), B (44–50 ppm), Na (35–53 ppm), Li (16–33 ppm), Mg (4–7 ppm), Sc (6–7 ppm), and Sn (3–10 ppm). Overall we observe that these quartzes are devoid of chromophore elements such as Fe, Mn, and Ti (below detection limits). Furthermore, in accordance with the previous models in the literature, a good correlation is observed between the concentration of monovalent cations (Li + Na) and those of Al. Al is the only trace substituent of Si, while Li and Na are interstitial elements that act as

charge compensators. Finally, a relevant quantity of hafnium is found, the origin of which is difficult to establish.

Table 2. Trace element composition of the quartz investigated in this work, obtained through LA-ICP-MS analysis (three spots per sample; the values in table are the averages). The elements that resulted below the detection limits (bdl) are not reported; detection limits are reported in [40].

Trace Element Concentrations (ppmw) SDD (Limits of Detection)						
Element	Qz 1	Qz 2	Qz 3	Qz 4	Qz 5	
⁷ Li	18.92	25.6	31.69	16.48	33.47	7.52
¹¹ B	44.46	45.94	44.12	45.99	50.54	2.56
²³ Na	36.61	35.68	53.09	36.63	36.38	7.51
²⁵ Mg	3.9	2.89	6.97	4.16	3.98	1.53
²⁷ Al	194.49	248.27	352.12	241.14	342.18	68.56
Si (%)	99.8	99.8	99.8	99.8	99.8	
⁴⁵ Sc	7.41	7.62	6.96	5.84	6.56	0.71
¹¹⁸ Sn	3.3	6.19	6.23	2.85	9.54	2.70
¹⁷⁷ Hf	45.32	79.69	bdl	31.23	90.41	28.85

5. Discussion and Conclusions

The analyses carried out in this work allowed for the estimation of the gemological properties of black quartz, to better understand their geologic origin and the causes of their dark color. The euhedral quartz crystals include many different types of inclusions—according to our observations and those reported in [6,41], the solid ones are composed mostly of disordered graphite and anhydrite. Gypsum inclusions are absent, even in quartz crystals hosted in gypsum rich rocks and into evaporite-free residual deposits. The widespread presence of these anhydrite inclusions would indicate that the sulphate deposits, during the growth of the quartz, were mainly composed of anhydrite. However, experimental studies and observations on current evaporite deposits [42,43] have shown that anhydrite has little chance of precipitating in submarine evaporitic environments; consequently, the most common precipitate in Triassic marine waters was gypsum, not anhydrite. It can therefore be hypothesized that during the tectonic processes that affected the northern Apennine chain, the syn-depositional gypsum was dehydrated and converted into anhydrite, due to the increase in geothermal temperatures that referred to the increase in the depth of the burial. As a matter of fact, the transformation of gypsum into anhydrite due to increasing burial temperatures explains the general absence of gypsum at depths greater than 1000 m, while anhydrite is always present. This hypothesis agrees with the model of the tectonic evolution of the Burano Formation that was buried by the 2000 m-thick carbonate sequence of the Tuscan Nappe during the Cretaceous [44]. Subsequently, the exhumation and denudation of the Burano Formation produced a complete hydration of anhydrite rocks, which were converted into gypsum. The solid inclusions in the euhedral quartz crystals, therefore, provide further evidence for the geologic evolution of the Burano and correspond to the Apuan metamorphic complex of green schist facies [45]. We can therefore hypothesize that quartzes are authigenic and formed in the Oligocene–Miocene during the burial of the evaporitic formation, when gypsum converted into anhydrite. The absence of elements such as Ti, K, and Fe (bdl) and the transition elements would exclude magmatic genesis. We believe that quartz was formed from high salinity fluids, produced by an increase in pressure and temperature inside the evaporites; the assumed temperature during this process is about 260–300 °C [46–51]. The fluids would have solubilized the organic silica of the microorganisms contained in the evaporitic bodies, subsequently redepositing it as idiomorphic quartz in the surrounding anhydrites. In fact, it is known that diatoms with a siliceous shell live in waters with very variable

salinities, but always at low depths, as in the photic zone. A possible confirmation of this origin of the fluids is given by the considerable presence of Hf inside the quartz crystals, as this element is present in various types of sediments, especially organic, according to the literature [52–54]. In fact, the solubility of Hf in fluids, generally modest, increases when the Hf enters complexes containing sulfate, arsenate, but above organic anions. Another source of silica could be represented by the thin layers of detrital silt, up to 50 cm thick, interspersed in the Burano Formation, which are mainly composed of quartz, muscovite, illite, chlorite, and feldspar [41]. Our analyses also allowed us to ascertain the causes of the black color of the quartz, which is not to be attributed to the chromophores, as they are present in very low quantities. [33,35,36]. We believe that the black color is not even to be attributed to the color centers, as in the case of the smoky quartz, as even after heating (280 °C/2 h, in an oxidizing atmosphere), the color of our samples remains dark, while the color centers should disappear after this treatment [1,3,55]. Additionally, smoky quartz crystals exhibit a vitreous luster, while our crystals exhibit a distinct metallic luster and opaque appearance due to the presence of graphite. Consequently, the dark color should be attributed to the disordered graphite inclusions previously described. The color of the samples becomes darker and more intense with the increase of these inclusions; therefore, these quartzes should be called black and not smoky quartz. However, it must be emphasized that, according to some articles, the polishing operations could alter the graphitic carbon, and consequently the Raman spectra may not be really representative of the composition of the inclusions [32–34]. Consequently, we believe the exact nature of these inclusions will need to be further investigated by other techniques like UV-Vis [56]. The chromatic inhomogeneity of these gems is instead to be attributed to the presence of large anhydrite inclusions.

The black quartzes of the Burano Formation represent an appreciable gemological material. Unfortunately, however, the difficulties in reaching the deposit limit the marketing of these quartzes, which are well known by Italian and European collectors. Furthermore, the locality is a protected park in the Emilia Romagna region, which, to safeguard the eco-sustainability of quartz extraction, grants permission only to goldsmiths. In Italy, a significant problem in recent decades has been the abandonment by local populations of mountain areas such as the Apennines and the Alps. In fact, for reasons of comfort of life and job opportunities, the younger generations leave the regions of the mountains to move to the cities of the plains, but this generates significant social and environmental problems; moreover, these small towns of the Apennines are considered among the most typical and beautiful elements of Italy. To stem this phenomenon and encourage young people to stay in their villages, it is necessary to create new cultural interests and job opportunities that are sustainable from an environmental point of view. We think that encouraging local artisanship of precious stones can be a valid help in this direction, as long as the extraction of the stones is done manually and in a strictly controlled manner. We also suggest creating a geopark for educational and informative purposes, which can also be combined with agrotourism activities.

Author Contributions: Conceptualization, F.C. and M.S.; methodology, F.C. and M.G.; software, M.S.; validation, all the authors; formal analysis, F.C. and M.G.; investigation and data curation, all the authors; writing—original draft preparation, F.C., M.S. and L. M.; writing—review and editing, F.C., M.S. and L.M.; visualization and supervision, all the authors. All authors have read and agreed to the published version of the manuscript.

Funding: This research received no external funding.

Acknowledgments: The authors are grateful to Antonio Langone for the LA-ICP-MS analyses, to Omar Bartoli for the thin section, and to Antonio Miglioli (Sassuolo, Mo), Enrico Borghi (Re), and Enrico Bonacina (Bg) for several images.

Conflicts of Interest: The authors declare no conflict of interest.

References

1. Caucia, F.; Ghisoli, C. *Quarzi: Definizione, Nomenclatura e Proposta di Classificazione Delle Varietà*; Museo Civico di Storia Naturale Cremona: Cremona, Italy, 2004; p. 259.
2. Scacchetti, M.; Bartoli, O.; Bersani, D.; Laurora, A.; Lugli, S.; Malferrari, D.; Valeriani, L. *Minerali della provincia di Reggio Emilia*; AMI Cremona: Cremona, Italy, 2015; p. 256.
3. Hatipoğlu, M.; Helvacı, C.; Kibar, R.; Çetin, A.; Tuncer, Y.; Can, N. Amethyst and morion quartz gemstone raw materials from Turkey: Color saturation and enhancement by gamma, neutron and beta irradiation. *Radiat. Eff. Defects Solids* **2010**, *65*, 876–888. [[CrossRef](#)]
4. Available online: <https://www.geologyin.com/2020/02/is-black-quartz-natural.html> (accessed on 3 August 2022).
5. Available online: <https://www.mindat.org/loc-22957.html> (accessed on 3 August 2022).
6. Lugli, S. Petrography of the quartz euhedral as a tool to provide indications on the geologic history of the Upper Triassic Burano Evaporites (Northern Apennines). *Mem. Soc. Geol. It.* **1994**, *48*, 61–65.
7. Lugli, S. La storia geologica dei gessi triassici della Val Secchia. *Ist. It. Spel. Mem.* **2009**, *22*, 25–36.
8. Vighi, L. Sulla serie triassica “Cavernoso-Verrucano” presso Capalbio (Orbetello—Toscana) e sulla brecciatura tettonica delle serie evaporitiche, “Roccmadri” del Cavernoso. *Boll. Della Soc. Geol. Ital.* **1958**, *78*, 221–236.
9. Ciarapica, G.; Passeri, L. Deformazioni da fluidificazione ed evoluzione diagenetica della formazione evaporitica di Burano. *Boll. Della Soc. Geol. Ital.* **1976**, *95*, 1175–1199.
10. Ciarapica, G.; Cirilli, S.; Passeri, L.; Trincianti, E.; Zaninetti, L. “Anidriti di Burano” et “Formation du Monte Cetona” (nouvelle formation), biostratigraphie de deux series-types du Trias superieur dans l’Apennin septentrional. *Rev. Paleobiol.* **1987**, *6*, 341–409.
11. Martini, R.; Gandin, A.; Zaninetti, L. Sedimentology, Stratigraphy and micropaleontology of the Triassic evaporitic sequence in the subsurface of Boccheggiano and in some outcrops of southern Tuscany (Italy). *Riv. Ital. Paleontol. Stratigr.* **1989**, *95*, 3–28.
12. Regione Emilia Romagna. *Note Illustrative Della Carta Geologica D’ITALIA Alla Scala 1:50.000, Foglio 235, Pievepelago*; Selca: Firenze, Italy, 2002; p. 140.
13. Colombetti, A.; Fazzini, P. Il salgemma nella formazione dei gessi triassici di Burano (Villaminazzo, RE). *Grotte D’italia* **1986**, *4*, 209–219.
14. Forti, P.; Francavilla, F.; Prata, E.; Rabbi, E.; Chiesi, M. Hydrogeology and hydrogeochemistry of the triassic evaporite in the upper Secchia valley (Reggio Emilia, Italy) and the Poiano karst spring. *Grotte D’italia* **1986**, *4*, 267–278.
15. Lugli, S.; Parea, G.C. Halite cube casts in the Triassic sandstones from The Upper Secchia River valley (Northern Apennines, Italy): Environmental interpretation. *Accad. Naz. Sci. Lett. Arti Modena* **1996**, *15*, 341–351.
16. Lugli, S.; Morteani, G.; Blamart, D. Petrographic, REE, fluid inclusion and stable isotope study of the magnesite from the Upper Triassic Burano Evaporites (Secchia Valley, northern Apennines): Contributions from sedimentary, hydrothermal and metasomatic sources. *Miner. Depos.* **2002**, *37*, 480–494. [[CrossRef](#)]
17. Bertolani, M.; Rossi, A. La petrografia del “Tanone grande della Gaggiolina” (154 E/RE) nelle evaporiti dell’Alta Val Secchia (Reggio Emilia—Italia). *Grotte D’italia* **1986**, *4*, 79–105.
18. Chiesi, M.; Forti, P. Le sorgenti carsiche di Poiano. *Ambiente Nat. Po Degli Appennini* **1987**, *3*, 11–15.
19. Lugli, S.; Domenichini, M.; Catellani, C. Peculiar karstic features in the Upper Triassic sulphate evaporites from the Secchia Valley (Northern Apennines, Italy). In *Gypsum Karst Areas in the World, Their Protection and Tourist Development*. Bologna, 26 Agosto 2003; Istituto Italiano di Speleologia, Memoria: Bologna, Italy, 2004; Volume XVI, pp. 99–106.
20. Colombetti, A.; Zerilli, A. Prime valutazioni dello spessore dei gessi triassici mediante sondaggi elettrici verticali nella Valle del F. Secchia (Villa Minozzo- R.E.). *Mem. Soc. Geol. Ital.* **1987**, *39*, 83–90.
21. Andreozzi, M.; Casanova, S.; Chicchi, S.; Ferrari, S.; Patterlini, P.; Pesci, M.; Zanzucchi, G. Riflessioni sulle evaporiti triassiche dell’alta Val Secchia (RE). *Mem. Soc. Geol. Ital.* **1987**, *39*, 69–75.
22. Chicchi, S.; Plesi, G. Sedimentary and tectonic lineations as markers of regional deformation: An example from the Oligo-Miocene arenaceous Flysch of the Northern Apennines. *Boll. Soc. Geol. Ital.* **1991**, *110*, 601–616.
23. Chicchi, S.; Costa, E.; Lugli, S.; Molli, G.; Montanini, A.; Torelli, L.; CavoZZi, C. The Passo del Cerreto-Val Secchia evaporites and associated rocks. In Proceedings of the Field trip guide book Realmod Conference San Donato Milanese (MI), San Donato Milanese, Italy, 2–4 October 2002.
24. Available online: https://www.rapidtables.com/web/color/RGB_Color.html (accessed on 3 August 2022).
25. Laughner, J.W.; Newnham, R.E.; Cross, L.E. Mechanical Twinning in small quartz crystals. *Phys. Chem. Miner.* **1982**, *8*, 20–24. [[CrossRef](#)]
26. Grimm, W.D. Idiomorphe Quarze als Leit mineralien für salinare Fazies. *Erdöl Kohle* **1962**, *15*, 880–887.
27. Tarr, W.A. Doubly terminated quartz crystals occurring in gypsum. *Am. Miner.* **1929**, *14*, 19–25.
28. Etchepare, J.; Merian, M.; Smetankine, L. Vibrational normal modes of SiO₂. I. α and β quartz. *J. Chem. Phys.* **1974**, *60*, 1873. [[CrossRef](#)]
29. Liu, Y.; Wang, A.; Freeman, J. Raman, MIR and NIR spectroscopic study of calcium sulfates: Gypsum, bassanite and anhydrite. In Proceedings of the 40th Lunar and Planetary Science Conference, The Woodlands, TX, USA, 23–26 March 2009.
30. Bagavantam, S.; Venkatara, T. The normal modes and frequencies of the sulphur molecule. In *Proceedings of the Indian Academy of Science, Section A*; Springer: Berlin/Heidelberg, Germany, 1938; pp. 101–114.

31. Loun, J.; Cejka, J.; Sejkora, J.; Plasil, J.; Novak, M.; Frost, R.; Palmer, S.; Keeffe, E.A. Raman spectroscopic study of bukovskyite $\text{Fe}_2(\text{AsO}_4)(\text{SO}_4)(\text{OH}) \cdot 7\text{H}_2\text{O}$, a mineral phase with a significant role in arsenic migration. *J. Raman Spectrosc.* **2011**, *42*, 1596–1600. [[CrossRef](#)]
32. Pimenta, W.M.A.; Dresselhaus, G.; Dresselhaus, M.S.; Cancado, L.G.; Jorio, A.; Saito, R. Studying disorder in graphite-based systems by Raman spectroscopy. *Phys. Chem.* **2007**, *9*, 1276–1291. [[CrossRef](#)] [[PubMed](#)]
33. Ferrari, A.C. Raman spectroscopy of graphene and graphite: Disorder, electron–phonon coupling, doping and nonadiabatic effects. *Solid State Commun.* **2007**, *143*, 47–57. [[CrossRef](#)]
34. Escribano, R.; Sloan, J.J.; Siddique, N.; Sze, N.; Dudev, T. Raman spectroscopy of carbon-containing particles. *Vib. Spectrosc.* **2001**, *26*, 179–186. [[CrossRef](#)]
35. Jehlička, J.; Urban, O.; Pokorný, J. Raman spectroscopy of carbon and solid bitumens in sedimentary and metamorphic rocks. *Spectrochim. Acta Part A Mol. Biomol. Spectrosc.* **2003**, *59*, 2341–2352. [[CrossRef](#)]
36. Potgieter-Vermaak, S.; Maledi, N.; Wagner, N.; Van Heerden, J.H.P.; Van Grieken, R.; Potgieter, J.H. Raman spectroscopy for the analysis of coal: A review. *J. Raman Spectrosc.* **2011**, *42*, 123–129. [[CrossRef](#)]
37. Available online: <http://rruff.info/graphiteR050503> (accessed on 3 August 2022).
38. Available online: <http://rruff.info/anhydriteR040012> (accessed on 3 August 2022).
39. Available online: <http://rruff.info/quartzR04001> (accessed on 3 August 2022).
40. Miller, C.; Zanetti, A.; Thoni, M.; Konzett, J.; Klotzli, U. Mafic and silica-rich glasses in mantle xenoliths from Wau-ennamus, Lybia: Textural and geochemical evidence for peridotite melt reactions. *Lithos* **2012**, *128*, 11–26. [[CrossRef](#)]
41. Lugli, S.; (Chemical and Geological Department, University of Modena and Reggio Emilia, Italy). Personal Communication, 2012.
42. Lugli, S. Timing of post-depositional events in the Burano Formation of the Secchia valley (Upper Triassic, Northern Apennines), clues from gypsum–anhydrite transitions and carbonate metasomatism. *Sediment. Geol.* **2001**, *140*, 107–122. [[CrossRef](#)]
43. Schreiber, B.C. Arid shorelines and evaporites. In *Sedimentary Environments and Facies*; Reading, H.G., Ed.; Blackwell: Oxford, UK, 1986; pp. 128–189.
44. Shearman, D.J. Syn-depositional and late diagenetic alteration of primary gypsum to anhydrite. In *Sixth International Symposium on Salt*; Schreiber, B.C., Ed.; Salt Institute: Portland, ME, USA, 1985; Volume 1, pp. 41–55.
45. Boccaletti, M.; Decandia, F.A.; Gasperi, G.; Gelmini, R.; Lazzarotto, A.; Zanzucchi, G. *Note Illustrative Della Carta Strutturale dell'appennino Settentrionale*; CNR, Progr. Finalizzato Geodinamica; Consiglio Nazionale delle Ricerche, Progetto Finalizzato Geodinamica, Sottoprogetto: Siena, Italy, 1987; Volume 429, p. 203.
46. Murray, R.C. Origin and diagenesis of gypsum and anhydrite. *J. Sed. Geol.* **1964**, *34*, 512–523.
47. Lugli, S. Petrography and geochemistry of the Upper Triassic Burano Evaporites (Northern Apennines, Central Italy). *Plinius* **1993**, *9*, 87–92.
48. Lugli, S. The magnesite in the Upper Triassic Burano Evaporites of the Secchia River valley (Northern Apennines, Italy): Petrographic evidence of an hydrothermal-metasomatic system. *Mem. Soc. Geol. Ital.* **1996**, *48*, 669–674.
49. Lugli, S. Megabrecce solfatiche nella Formazione di Burano dell'alta val di Secchia (Trias sup., RE): Cap rock da dissoluzione di salgemma. In Proceedings of the 1° Forum Italiano di Scienze della Terra, Geoitalia, Bellaria, Rimini, Italy, 5–9 October 1997; Volume 2, pp. 36–38.
50. Carmignani, L.; Kligfield, R. Crustal extension in the northern Apennines: The transition from compression to extension in the Alpi Apuane core complex. *Tectonics* **1990**, *9*, 1275–1303. [[CrossRef](#)]
51. Mc Lennan, S.; Murray, S.R. Earth's continental crust. In *Encyclopedia of Geochemistry*; Marshall, C.P., Fairbridge, R.W., Eds.; Kluwer: Dordrecht, The Netherlands, 1999; pp. 145–151.
52. Vlasov, K.A. Geochemistry and Mineralogy of rare Elements and genetic types of their deposits. In *I Geochemistry of Rare Elements(a), II Mineralogy of Rare Elements (b)*; Israel Program for Scientific Translations: Jerusalem, Israel, 1966.
53. Kabate Pendas, A.; Szeke, B. *Hafnium [Hf, 72] In Trace Elements in Abiotic and Biotic Environments*; CRC Press: Boca Raton, FL, USA, 2015; 3p.
54. Taylor, A.; Mc Lennan, S. The geochemical evolution of the continental crust. *Rev. Geophys.* **1995**, *33*, 241–265. [[CrossRef](#)]
55. Spingardi, A. Analyses of Charge Transfer and Color Centers in Gem-Quality Minerals with Thermal Treatment. Master's Thesis, Università di Pavia, Pavia, Italy, 2006; p. 164.
56. Beysac, O.; Lazzeri, M. Application of Raman Spectroscopy to the study of graphitic carbon in the earth Sciences. *Eur. Mineral. Union Notes Mineral.* **2012**, *12*, 415–454.